Catalysis Today 139 (2008) 174–179

Contents lists available at ScienceDirect

Catalysis Today

journal homepage: www.elsevier.com/locate/cattod

Support effect on the catalytic performance of $Au/Co_3O_4–CeO_2$ catalysts for CO and CH_4 oxidation

L.F. Liotta [a], G. Di Carlo [b], A. Longo [a], G. Pantaleo [a], A.M. Venezia [a,*]

[a] Istitusto per lo Studio di Materiali Nanostrutturati, CNR, Via Ugo La Malfa, 153, 90146 Palermo, Italy
[b] Dipt. Chimica Inorganica e Analitica, "S. Cannizzaro", Università di Palermo, V.le delle Scienze, Parco D'Orleans, 90128 Palermo, Italy

ARTICLE INFO

Article history:
Available online 9 June 2008

Keywords:
Au catalysts
$Co_3O_4–CeO_2$ supports
CO and CH_4 oxidation
SO_2 effect

ABSTRACT

Gold-based catalysts supported on Co_3O_4, on CeO_2 and on mixed $Co_3O_4–CeO_2$ oxides were prepared by co-precipitation. They were tested in the catalytic oxidation of CO and CH_4, in separate tests, and their activities were compared with that of the bare oxides. Tests of CH_4 oxidation were performed in two consecutive runs in order to evaluate the catalysts stability. The effect of SO_2 in the reactant mixture was investigated. The fresh and spent catalysts were analsed by XRD, BET, TPR and XPS techniques. Among the fresh catalysts, Au supported on CeO_2 was the most active in CO oxidation whereas Au supported on Co_3O_4 was the most active for methane total oxidation. Synergy between the two oxides was not observed for gold on mixed $Co_3O_4–CeO_2$ system. However, in consecutive runs of methane oxidation and in the presence of SO_2, Au supported on mixed $Co_3O_4–CeO_2$ exhibited higher stability and superior SO_2 tolerance as compared to the single oxide catalysts.

1. Introduction

Cold-start emissions are responsible for ~80% of the pollution emitted by gasoline vehicles, since conventional three way catalysts are not efficient at temperatures below 200 °C [1]. Carbon monoxide and unburned hydrocarbons are the main pollutants emitted during the cold-start operation. In order to comply with the new limits imposed by the legislation on pollution control, more efficient catalysts are needed. Recently, the catalytic combustion of alkanes, especially methane [2], has received particular attention due to the increasing use of lean burn natural gas vehicles (NGVs) [3]. Both classes of catalysts, metal oxides [4–6] and noble metals [7–9] are currently explored for this process. The noble metals, particularly Pd and Pt, are the preferred ones because of their high specific activity [10]. They are used in current commercial catalysts for cleaning exhausts from NGVs [11,12]. However, sulfur compounds, present as impurities or odorizer in the natural gas and/or in the lubricating oil cause serious deactivation of both Pt and Pd catalysts [2,7].

Gold has historically been considered an inert element. However, since the discovery of the high activity exhibited by supported gold particles of sizes 3–5 nm, in CO oxidation at low temperature, the interest in using gold as a catalyst component has increased enormously [13]. Recently, gold in combination with platinum and palladium, was used as an automotive catalyst [14]. The application of supported gold catalysts for the total oxidation of hydrocarbons and carbon monoxide has been addressed in several papers [15–19]. In particular, Au/Co_3O_4 was recognized as one of the most active catalyst for methane oxidation, among a series of coprecipitated Au on several transition metal oxides [15]. Moreover, the structural promotion by CeO_2 of a Co_3O_4 catalyst was observed in methane total oxidation [20,21]. The positive effect was attributed to an improved thermal stability, and an increased dispersion of the active phase.

Aiming to explore the reciprocal effect of gold and mixed oxide system $Co_3O_4–CeO_2$, coprecipitated catalysts of gold on Co_3O_4, CeO_2 and mixed oxides were prepared, characterised by XRD, BET, TPR, XPS and tested in the CO and CH_4 oxidation. During the oxidation of CH_4, the effect of SO_2 in the reaction feed was evaluated.

2. Experimental

2.1. Catalyst preparation

The catalysts $AuCo_3O_4$, $AuCeO_2$ and $AuCo_3O_4–CeO_2$ (thereafter labelled as AuCoCe, with Co:Ce atomic ratio 1:1) were prepared by co-precipitation method, according to a published procedure [21]. An appropriate volume of $HAuCl_4$ water solution to yield a final 10 wt% Au loading and the calculated amounts of cobalt and

* Corresponding author.
E-mail address: anna@pa.ismn.cnr.it (A.M. Venezia).

0920-5861/$ – see front matter © 2008 Elsevier B.V. All rights reserved.
doi:10.1016/j.cattod.2008.04.025

cerium nitrates were mixed. Aqueous Na_2CO_3 0.25 M as precipitating agent was added drop-wise until a pH of 8.5 was attained. The resulting precipitate was aged at room temperature for 3 h, then filtered, washed several times with hot water and dried at 120 °C overnight. The obtained samples were calcined at 400 °C for 4 h and then at 600 °C for 1 h. For comparison, corresponding bare oxides Co_3O_4, Co_3O_4–CeO_2 (indicated as CoCe) and CeO_2 were also prepared by co-precipitation method and were calcined at the same temperature as the gold catalysts.

2.2. Catalyst characterization

The X-ray diffraction analyses were carried out with a Philips vertical goniometer using Ni-filtered Cu Kα radiation (λ = 1.5418 Å). The spectra were collected with a step size of 0.05° and a counting time of 10 s per angular abscissa. The XRD profiles were reproduced using Rietveld refinement [22], in order to estimate the modification of the crystalline phases upon catalytic tests. The fit goodness was ascertained by low values (≤0.03) of R_p and R_{wp} [22]. The assignment of the various crystalline phases was based on the ICSD data base (Au, no. 58393; Co_3O_4, no. 24210; CoO, no. 9865; CeO_2, no. 28785) [23]. The fittings were performed by the GSAS package program and the particle sizes were determined, with an error of ±2%, using the Scherrer equation on the basis of the calculated Lorentzian broadening [24,25].

The specific surface areas were determined by BET method [26] from nitrogen adsorption isotherms at −196 °C using Sorptomatic 1900 (Carlo Erba) instrument.

The X-ray photoelectron spectroscopy analyses were performed with a VG Microtech ESCA 3000 Multilab, using the unmonochromatised Al Kα source (1486.6 eV) run at 14 kV and 15 mA. For the individual peak energy regions, a pass energy of 20 eV was used. Samples were mounted with double-sided adhesive tape. Binding energies were referenced to the C 1s binding energy of adventitious carbon set at 285.1 eV. The software provided by VG was used for peak analyses and for the calculation of the atomic concentrations. The precision on the binding energy and on the atomic percentage values were respectively ±0.15 eV and ±10%.

2.3. Catalytic activity

Catalytic tests were performed using a *U*-shaped quartz reactor with an inner diameter of 12 mm, electrically heated in a furnace. The catalyst powder (sieved fraction between 180 and 250 μm) was diluted 1:2 with inert SiC in order to avoid thermal gradients and it was placed on a porous quartz disk. The reaction temperature was measured by a K-type thermocouple in contact with the catalytic bed 12 mm long. Prior to the catalytic testing, the samples were treated "in situ" under flowing O_2 (5 vol.% in He, 50 ml/min) at 350 °C for 1/2 h and in He during cooling to room temperature. The standard reagent gas mixture consisting of 1 vol.%CO + 1 vol.%O_2 in He or 0.3 vol.%CH_4 + 2.4 vol.%O_2 in He was led over the catalyst (50 mg) at a flow rate of 50 ml/min (STP), equivalent to a weight hourly space velocity (WHSV) of 60,000 ml g^{-1} h^{-1}. In order to assess the stability of the catalysts, two reaction runs were recorded consecutively, the first one from r.t. up to 600 °C, the second one up to 800 °C, keeping the catalyst under the reaction mixture during the cooling. The performance of the catalysts in both reactions is given in terms of the temperature corresponding to 50% conversion. For general comparison purpose pseudo-first order reaction rates were also calculated using differential reactor equation.

The inlet and outlet gas compositions were analyzed by on line mass quadrupole (Thermostar™, Balzers), in order to follow the evolution of all the species, CH_4, CO, CO_2, H_2, H_2O and O_2. Moreover, the concentration of CO and CO_2 was checked by an IR analyser (ABB Uras 14), calibrated in the range of 0–3000 ppm for CO and 0–10,000 ppm for CO_2. The reaction products of methane oxidation were CO_2 and H_2O. No CO was detected in the overall range of temperature. Carbon balance was close to ±5% in all the catalytic tests. Experiments of methane oxidation in presence of SO_2 were performed by co-feeding 10 vol ppm of SO_2.

3. Results and discussion

3.1. Catalytic activity

In Fig. 1 the CO conversion as a function of the temperature is displayed for Au supported catalysts and for the supports. In Table 1 the temperatures in correspondence of 50% CO conversion (T_{50}) and the specific reaction rates calculated at low conversion (at 70 °C) over Au supported catalysts and the corresponding bare oxides are listed. It is worth noticing that the supports containing cobalt are able to convert CO at temperature below 200 °C, differently from pure CeO_2 which starts to be active at higher temperature. Upon addition of gold the activity improves noticeably especially for the ceria supported catalyst. Among the catalysts, $AuCeO_2$ is the most active, followed by AuCoCe, and then by $AuCo_3O_4$. However, as expected, the activity of the co-precipitated gold ceria catalyst is lower with respect to the activity of a similar catalyst prepared by deposition-precipitation [27].

Light-off curves of methane oxidation in two consecutive runs are shown in Fig. 2. In Table 2 the temperatures of 50% methane conversion obtained with the gold catalysts and with the bare supports in different runs, together with the specific reaction rate calculated at low conversion (at 300 °C) for the 1st run, are listed. As for the CO oxidation, the presence of gold enhances the activity of the corresponding oxides. It is worth noting that, differently from the CO case, the activity of the Au catalysts changes as $AuCo_3O_4$ > AuCoCe > $AuCeO_2$, with the same trend as the activity of the corresponding oxides, suggesting a strong support effect. In the second run performed consecutively, a clear deactivation is observed, the extent of which strongly depends on the support. $AuCo_3O_4$ shows the most pronounced deactivation, with a T_{50} increase of 80 °C. Moreover, in accord with results from a study on similar oxides, a rapid deactivation due to the thermal decomposition of Co_3O_4 to the less active CoO occurs at $T > 700$ °C [21]. AuCoCe deactivates less in the second run with a T_{50} increase of

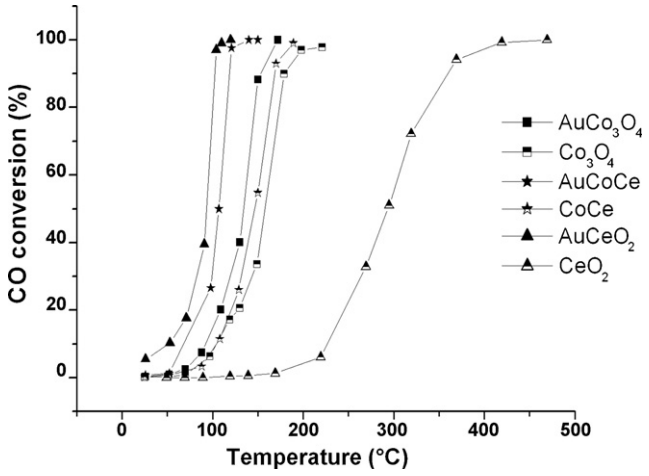

Fig. 1. CO conversion (%) as a function of the temperature for gold catalysts and the corresponding oxides.

Table 1
Temperature of 50% CO conversion T_{50} (°C) and specific reaction rate calculated at 70 °C over Au supported catalysts and the corresponding bare oxides

Sample	T_{50} (°C)	$r_{70\ °C}$ (μmol s^{-1} g^{-1}_{au})[a]
$AuCo_3O_4$	134	1.75
Co_3O_4	158	0.55
AuCoCe	106	3.64
CoCe	145	1.36
$AuCeO_2$	92	12.06
CeO_2	293	0

[a] The specific reaction rates are calculated at 70 °C.

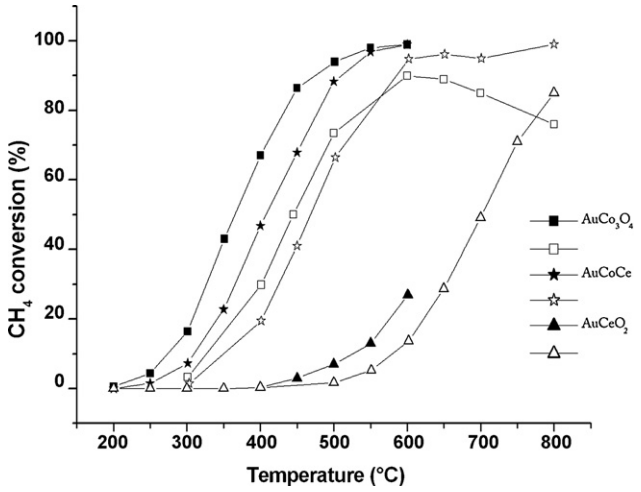

Fig. 2. Methane conversion curves versus temperature over gold supported catalysts: first and second runs (filled and open symbols, respectively).

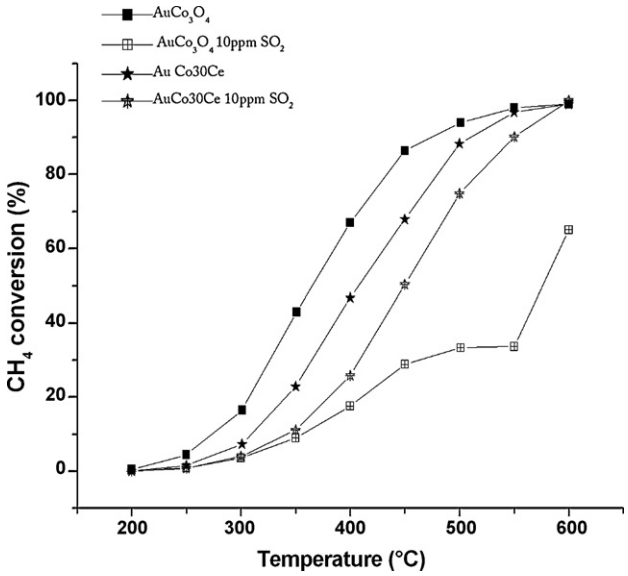

Fig. 3. Methane conversion curves versus temperature over $AuCo_3O_4$ and AuCoCe catalysts in presence of 10 ppm of SO_2 in the feed.

Table 3
Specific surface area (SSA) and XRD derived crystallite sizes (d) of the fresh gold catalysts

Catalyst	SSA_{BET} (m^2/g)	d_{Au} (nm)	$d_{Co_3O_4}$ (nm)	d_{CeO_2} (nm)
$AuCo_3O_4$	45	10	22	–
AuCoCe	47	9	9	5
$AuCeO_2$	41	8	–	7

60 °C, maintaining 70% of methane conversion at 500 °C and achieving 90% conversion at 600 °C. The activity of $AuCeO_2$ is too low for any practical interest.

In order to assess the potentiality of Co_3O_4-based catalysts for real application, the tolerance to sulfur poisoning of the fresh samples, $AuCo_3O_4$ and AuCoCe, was studied by co-feeding 10 vol ppm of SO_2 with the methane oxidation mixture. In Fig. 3 the curves of methane conversion versus temperature are compared to the corresponding curves of the SO_2-free runs. The results in terms of T_{50} are summarized in Table 2. The conversion curve of $AuCo_3O_4$ is characterised by a sort of plateau in the temperature range between 400 and 550 °C and reflects a strong deactivation with a T_{50} increase of more than 200 °C. The AuCoCe maintains a reasonably good activity with a T_{50} increase of only 44 °C. The different SO_2 effect may be ascribed to the nature of the oxide support. Indeed, in the coprecipitated $AuCo_3O_4$, as suggested by the data of Table 2, cobalt oxide plays an active role for CH_4 oxidation. In the presence of SO_2, as shown previously [28], Co_3O_4 would form a less active composite species $Co_3O_4(SO_x)$ which probably decomposes at temperature above 550 °C, causing the increase of the activity after the plateau in Fig. 3. On the other hand, the sulfating nature of ceria is well known, forming stable cerium sulfate [29]. On this basis, it may be concluded that upon exposure to SO_2 the preferential formation of cerium sulfate would limit the formation of the less active $Co_3O_4(SO_x)$ species which are predominant over $AuCo_3O_4$. In other words CeO_2 surface would function as chemical trap, thus removing quickly SO_2 from the feed stream and therefore preventing the Co or the gold phases to be irreversibly poisoned. These arguments are supported by recent findings about the improved tolerance to sulfur poisoning of cerium promoted Pd/Co_3O_4 catalyst [30].

3.2. Structural characterization

In Table 3 textural properties of the fresh catalysts are listed. In Fig. 4 the experimental and calculated XRD patterns of $AuCo_3O_4$, as fresh and after different catalytic tests are shown. Peaks attributed to cobalt oxides and to metallic Au are present. The Rietveld refinement allowed to estimate the particle sizes of Au and Co_3O_4 phases. The gold particle sizes range from 8 to 10 nm, slightly increasing from $AuCo_3O_4 < AuCoCe < AuCeO_2$. Similar surface areas, between 41 and 47 m^2/g, were obtained. Much larger

Table 2
Temperature of 50% CH_4 conversion T_{50} (°C) in different run conditions and specific reaction rate over Au supported catalysts and the corresponding bare oxides

Sample	1st run T_{50} (°C)	2nd run T_{50} (°C)	1st run with SO_2 T_{50} (°C)	r (μmol s^{-1} g^{-1}_{au})[a]
$AuCo_3O_4$	364	444	575	3.37
Co_3O_4	455	–	–	0.68
AuCoCe	405	465	449	1.50
CoCe	489	–	–	0.34
$AuCeO_2$	>600	699	–	0
CeO_2	719	–	–	0

[a] The specific reaction rates are calculated at 300 °C and refer to the 1st run without SO_2.

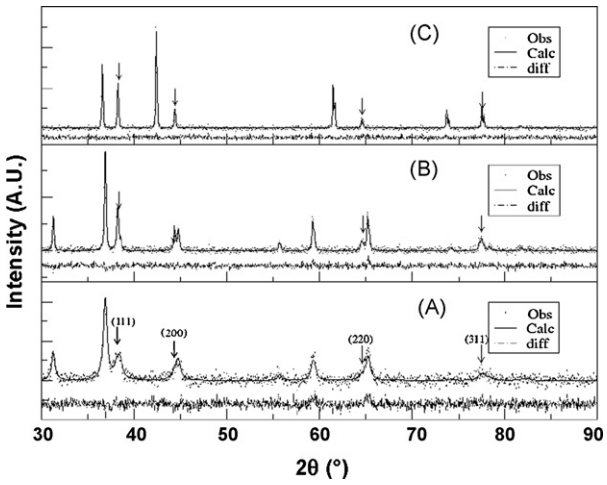

Fig. 4. Experimental and calculated (by Rietveld refinement) XRD patterns of $AuCo_3O_4$, as (A) fresh sample, (B) after first run up to 600 °C, (C) after second run up to 800 °C. The arrows indicate Au diffraction lines.

support crystallite sizes were found in the case of $AuCo_3O_4$ as compared to the mixed and CeO_2 supported Au catalysts. The structural analyses performed on the bare oxides allowed to conclude that the incorporation of gold did not modify substantially the surface area and the crystallite sizes of the corresponding oxides.

In order to get some insight in the deactivation process, XRD analyses were carried out over gold catalysts after methane oxidation tests. In Fig. 4(B) and (C) the experimental and calculated XRD patterns of $AuCo_3O_4$, after the first catalytic run, up to 600 °C, and after the second one, up to 800 °C, are displayed. The structural parameters calculated for $AuCo_3O_4$ and AuCoCe are listed in Table 4. $AuCo_3O_4$, upon two reaction cycles, undergoes a dramatic sintering of Au and Co_3O_4 crystallites, along with the complete decomposition of the Co_3O_4 phase into CoO, detected by the XRD after the second run. These structural modifications explain the observed deactivation of the catalyst during the second run as well as the activity decay in the range of 700–800 °C [16,31].

As shown from the data in Table 4 relative to the second run, AuCoCe is more stable with respect to Au particle sintering and Co_3O_4 decomposition. As previously reported, ceria stabilizes Au crystallites and prevents the complete decomposition of Co_3O_4 to CoO [32]. Similar effect was reported for Fe_2O_3 oxide which increased the stability of Co_3O_4 with respect to its reduction to CoO [33].

In Table 5 the XPS results in terms of Au $4f_{7/2}$, Co $2p_{3/2}$ and Ce $3d_{5/2}$ binding energies and Au/Co, Au/Ce atomic ratios, as obtained from XPS quantitative analyses, are reported. The experimental and fitted spectra of the Au 4f region of $AuCeO_2$, $AuCo_3O_4$ and

Table 4
Phases composition and calculated particle sizes (d) of aged $AuCo_3O_4$ and AuCoCe as obtained by Rietveld refinement

Catalyst	Phase	d (nm)
$AuCo_3O_4$	Au	21
After 1° run	Co_3O_4	55
$AuCo_3O_4$	Au	40
After 2° run	CoO	72
AuCoCe	Au	22
After 2° run	Co_3O_4	30
	CoO	28
	CeO_2	52

Table 5
XPS binding energies (eV) and surface atomic ratios of the fresh gold catalysts

Catalyst	Au $4f_{7/2}$ (eV)	Co $2p_{3/2}$ (eV)	Ce $3d_{5/2}$ (eV)	Au/Co	Au/Ce
$AuCo_3O_4$	84.5	779.5 780.9		0.03	
AuCoCe	84.6	779.1 780.9	881.4 883.5	0.03	0.05
$AuCeO_2$	84.5 (70%)[a] 85.8 (30%)		881.3 883.7		0.05

[a] The values represent the relative atomic percentages of the two Au components.

AuCoCe are shown in Fig. 5. The Au 4f ionization process is characterised by the doublet with the two spin–orbit components, Au $4f_{7/2}$ and Au $4f_{5/2}$ with a splitting of 3.7 eV. The position of the Au $4f_{7/2}$ component at 84.5 ± 0.1 eV, is at the typical binding energy value of metallic gold [27]. Only the $AuCeO_2$ exhibits an additional component at 85.8 eV typical of the oxidised species Au^+ [27,34]. In Fig. 6 the Co 2p spectra are shown. They are characterised by the spin orbit components Co $2p_{3/2}$ and Co $2p_{1/2}$ 15 eV apart. As for pure Co_3O_4, the broad and asymmetric spectra are fitted with the components arising from two cobalt species [4]. The Co $2p_{3/2}$ at 779.3 ± 0.3 eV is indicative of Co^{3+}, whereas the Co $2p_{3/2}$ at 780.9 eV associated with the shake up satellite is indicative of Co^{2+}. In Fig. 7 the experimental and fitted Ce 3d spectra of $AuCeO_2$ and AuCoCe are shown. The curves were fitted with eight peaks corresponding to four pairs of spin–orbit doublets. The labelling of the peaks follows the convention adopted by Burrough et al. [4,35]. Letters U and V refer to the $3d_{5/2}$ and $3d_{3/2}$ spin–orbit components, respectively. Three pairs of peaks (V,U; V'',U''; V''',U''') arise from different Ce 4f electron configuration in the final states of the Ce^{4+} species. The couple (V',U') corresponds to one of the two possible electron configuration of the final state of the Ce^{3+} species. The low and the high binding energy values of Ce $3d_{5/2}$ given in Table 5 are attributed to the component V and V' of Ce^{4+} and Ce^{3+}, respectively. No significant changes in the oxidation state of cobalt induced by the presence of ceria and viceversa seem to occur. X-ray photoelectron spectra of the gold catalysts after the second run were also collected. The data are summarized in Table 6. In accord with XRD results, the Co 2p spectra of $AuCo_3O_4$ exhibits only the Co $2p_{3/2}$ component at 780.5 eV with a strong shake-up satellite indicative of Co^{2+} only. In contrast to $AuCo_3O_4$, the Co 2p region of the AuCoCe

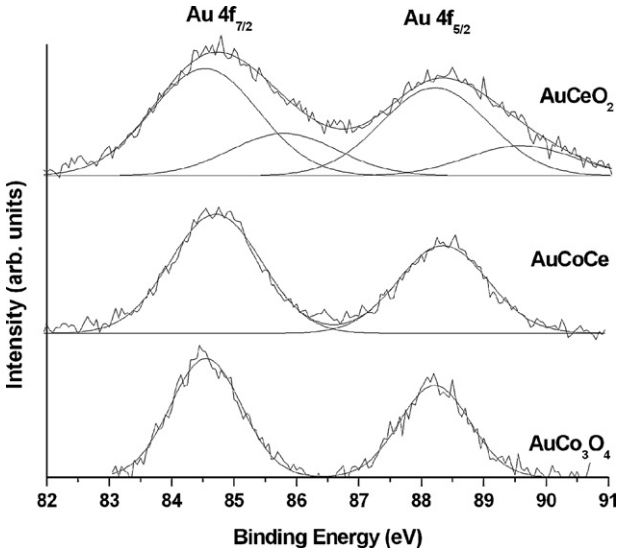

Fig. 5. Experimental and fitted Au 4f spectra of gold supported catalysts.

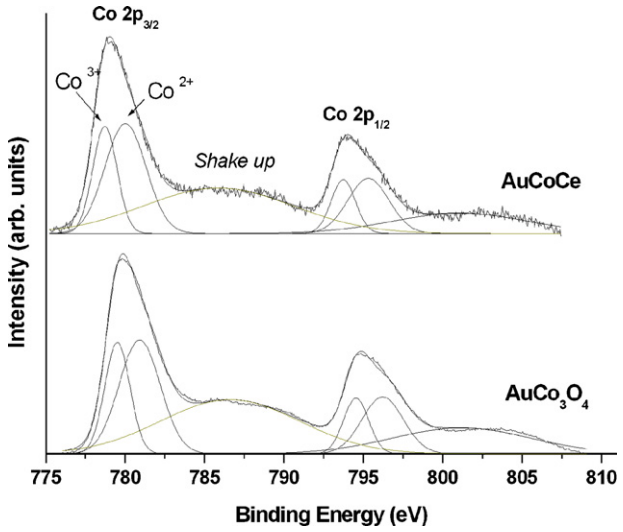

Fig. 6. Experimental and fitted Co 2p spectra of gold supported catalysts.

catalyst shows both Co^{2+} and Co^{3+} components. The surface Au/Co and Au/Ce atomic ratios before (Table 5) and after catalytic tests (Table 6) could be due to an enhancement of the gold surface dispersion or to sintering of the support phase. In accord with the XRD data the increased atomic ratios are likely due to the large increase of the support crystallite sizes.

To investigate the redox properties of the supports upon addition of gold, H_2-TPR experiments were carried out. The curves of the gold catalysts and of the corresponding supports are shown in Fig. 8. The profiles of gold catalysts differ from those of the corresponding bare supports depending on the type and strength of interaction of the metallic species with the carrier. The TPR profile of $AuCeO_2$ contains two peaks, one at 180 °C and the other at 780 °C associated with the surface and bulk reduction of ceria, respectively [27]. The maximum of the first peak is placed at significantly lower temperature than that of the surface CeO_2 (498 °C), in agreement with other studies which have shown that the presence of noble metal increases the reducibility of the support surface [36,37]. This effect was generally explained by the hydrogen spill-over from the metal to the support [38]. The maximum of the second peak (at 780 °C in the catalyst and at

Table 6
XPS data of $AuCo_3O_4$ and AuCoCe catalysts after catalytic tests

Catalyst	Au $4f_{7/2}$ (eV)	Co $2p_{3/2}$ (eV)	Au/Co	Au/Ce
$AuCo_3O_4$	84.6	780.5	0.09	
After 2°run				
AuCoCe	84.6	779.6	0.08	0.14
After 2°run		780.9		

810 °C in the pure ceria) is only slightly affected by the presence of gold. In this case, the high temperature reduction process is controlled by the slow bulk diffusion of the oxygen vacancies created at the oxide surface [39] and deposition of the noble metal has a little effect. According to literature [18], a shift to lower temperature is observed also for $AuCo_3O_4$ (peaks at 254 °C and 298 °C, respectively) as compared to the Au-free oxide (peaks at 289 and 343 °C). The two peaks in the reduction profile of Co_3O_4, generally designated as α and β, correspond to a two steps reduction process (Co_3O_4 to CoO and CoO to Co^0, respectively) [21,40]. The reduction profile of AuCoCe in the low-temperature region exhibits a peak at 180 °C as for gold over ceria, and a second strong peak centred at 250 °C. At 760 °C a small feature due to the reduction of bulk ceria is visible. By comparing the two curves of AuCoCe and of the bare CoCe, the presence of gold determines a shift of the low-temperature peaks of the support (a well defined peak centred at 250 °C and a broad signal around 300–400 °C) to lower temperature, the bulk reduction of ceria remaining unchanged. Moreover, the presence of CeO_2 in synergy with Co_3O_4 improves the low-temperature reducibility of the cobalt oxide in the CoCe sample with respect to pure Co_3O_4 [21]. At the same time, the reducibility of surface and bulk ceria is also enhanced as compared to pure CeO_2 [41]. In fact, as observed in Table 3, the reciprocal reduction of the two oxide crystallite sizes may contribute to the lowering of the reduction temperature.

Based on the above characterization results an explanation of the different catalytic behavior of the gold catalysts in CO and CH_4 oxidation reaction is attempted. $AuCeO_2$ is better performing in CO oxidation, while $AuCo_3O_4$ and AuCoCe are better in CH_4 oxidation. CeO_2 is well known for its oxygen storage capacity and the role of surface vacancies in activating the CO oxidation reaction over supported gold catalysts has been clearly demonstrated [42]. Moreover, the presence of Au^+ species is important for higher CO

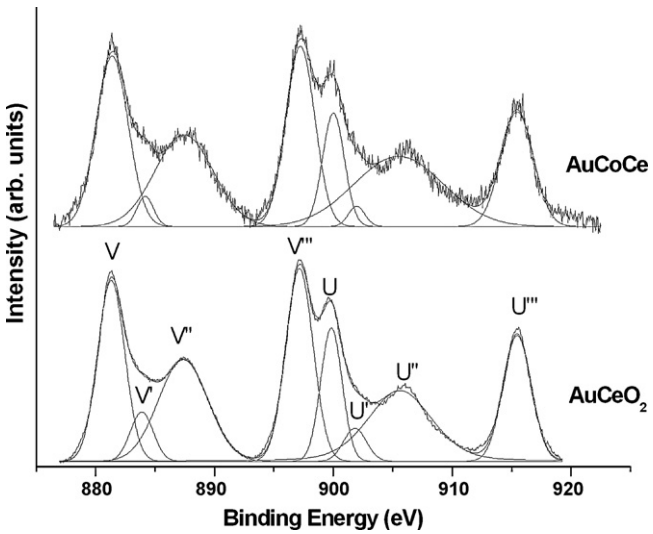

Fig. 7. Experimental and fitted Ce 3d spectra of gold supported catalysts.

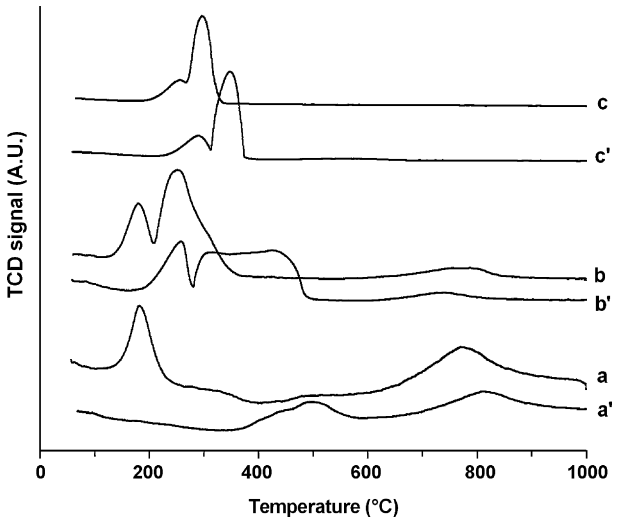

Fig. 8. H_2-TPR profiles of gold catalysts and the corresponding supports: (a) $AuCeO_2$; (a′) CeO_2; (b) AuCoCe; (b′) CoCe; (c) $AuCo_3O_4$; (c′) Co_3O_4.

conversion over $AuCeO_2$ catalysts [27,34]. Adding Co_3O_4 in the co-precipitation process, determines a slight increase of the gold particle size and most importantly, as seen from XPS, generates only metallic Au particles. These two effects may determine a lower CO oxidation activity of the Co containing samples. With respect to the oxidation of methane, it is generally accepted that in Co_3O_4-based catalysts, Co^{2+} ions in tetrahedral and Co^{3+} ions in octahedral coordination environment are active centres for adsorption of oxygen and hydrocarbons, respectively [43,44]. Accordingly, $AuCo_3O_4$ and AuCoCe perform better than $AuCeO_2$. Furthermore, the easy sintering of Au and Co_3O_4 crystallites contributes to the deactivation of the $AuCo_3O_4$. The presence of ceria in AuCoCe limits the process of particle aggregation. Moreover, due to the strong chemical interaction between CeO_2 and SO_2, forming a stable cerium sulfate, the presence of ceria increases the SO_2 tolerance during methane oxidation. Indeed, contrary to the $AuCo_3O_4$ which quickly deactivates, the AuCoCe maintains a good activity.

4. Conclusions

The comparative study of the CO and CH_4 oxidation over catalysts of Au supported on Co_2O_3, CeO_2 and mixed Co_2O_3–CeO_2 oxides, has shown a different support effect for the two reactions. The better performance of $AuCeO_2$ in low-temperature oxidation of CO is due to the peculiar oxygen mobility of ceria and to the presence of AuO^- species stabilized by cerium oxide. On the contrary, the better performance of the cobalt containing catalysts, $AuCo_3O_4$ and AuCoCe, in the methane oxidation reaction, is mainly attributed to the presence of Co^{2+} and Co^{3+} ions, being active sites for oxygen and methane activation, respectively. On the basis of the increased reducibility of the oxides, the beneficial effect of gold consists in the promotion of the oxygen mobility. The CeO_2 in AuCoCe plays the role of a structural promoter, limiting the Au sintering and the Co_3O_4 decomposition at temperature above $>600\ ^\circ C$. Furthermore, acting as a sort of SO_2 scavenger, by forming cerium sulfate, CeO_2 determines a superior SO_2 tolerance of the mixed AuCoCe catalyst.

Acknowledgements

Support by European Community, through the Network of Excellence (NoE) IDECAT (integrated Design of Catalytic Nanomaterials for a Sustainable Production) and COST D36 action is acknowledged.

References

[1] R.M. Heck, R.J. Farrauto, Catalytic Air Pollution Control, 2nd ed., John & Sons Inc., New York, 2002 (Chapter 6, p. 69).
[2] P. Gelin, M. Primet, Appl. Catal. B 39 (2002) 1.
[3] C.L. Battistelli, L. Conti, R. Crebelli, M. Gambino, A.L. Iamiceli, S. Iannaccone, L. Turrito Baldassarri, Evaluation of exhaust emission toxicity of heavy duty engines. ICE 2003, in: 6th International Conference on Engines for Automobile, September 14–19, 2003, Capri, Italy, 2003.
[4] L.F. Liotta, G. Di Carlo, G. Pantaleo, A.M. Venezia, G. Deganello, Appl. Catal. B 66 (2006) 217.
[5] N. Bahlawane, Appl. Catal. B 67 (2006) 168.
[6] T.V. Choudary, S. Banerjeem, V.R. Choudary, Appl. Catal. A 234 (2002) 1.
[7] J.K. Lampert, M.S. Kazi, R.J. Farrauto, Appl. Catal. B 14 (1997) 211.
[8] H. Yoshida, T. Nakajima, Y. Yazawa, T. Hattori, Appl. Catal. B 71 (2007) 70.
[9] A.M. Venezia, R. Muraria, G. Pantaleo, G. Deganello, J. Catal. 251 (2007) 94.
[10] R.M. Siewert, P.J. Mitchell, European Patent 0,468,556 A1 (1991).
[11] R.J. Farrauto, R.M. Heck, Catal. Today 51 (1999) 351.
[12] M. Gambino, S. Iannaccone, M.F. Pidria, G. Miletto, M. Rollero, Natural gas engine and catalyst deactivation: accelerated ageing tests, in: Proceedings of Fisita, World Automotive Congress, May 23–27, 2004, Barcelona, 2004.
[13] M. Haruta, S. Tsubota, T. Kobayashi, H. Kageyama, M.J. Genet, B. Delmon, J. Catal. 144 (1993) 175.
[14] Nanostellar Inc., Focus on Catalysts, June 2007.
[15] R.D. Waters, J.J. Weimer, J.E. Smith, Catal. Lett. 30 (1995) 181.
[16] R.J.H. Grisel, B.E. Nieuwenhuys, Catal. Today 64 (2001) 69.
[17] A.C. Gluhoi, N. Bogdanchikova, B.E. Nieuwenhuys, J. Catal. 232 (2005) 96.
[18] B.E. Solsona, T. Garcia, C. Jones, S.H. Taylor, A.F. Carley, G.J. Hutchings, Appl. Catal. A 312 (2006) 67.
[19] A.C. Gluhoi, B.E. Nieuwenhuys, Catal. Today 122 (2007) 226.
[20] L.F. Liotta, G. Di Carlo, G. Pantaleo, G. Deganello, Catal. Commun. 6 (2005) 329.
[21] L.F. Liotta, G. Di Carlo, G. Pantaleo, A.M. Venezia, G. Deganello, Appl. Catal. B (2006) 217.
[22] H.M. Rietveld, J. Appl. Cryst. 15 (1982) 357.
[23] Inorganic Crystal Structure Data Base (ICSD), National Institute of Standards and Technology (NIST), release 2007/2.
[24] H.P. Klug, X-ray Diffraction Procedure for Polycrystalline and Amorphous Materials, Wiley, New York, 1954.
[25] A. Larson, R.B. Von Dreele, Report LAUR 86-748, Los Alamos Laboratory, Los Alamos, NM (1988).
[26] S.J. Gregg, K.S. Sing, Adsorption Surface Area and Porosity, 2nd ed., Academic Press, San Diego, 1982.
[27] A.M. Venezia, G. Pantaleo, A. Longo, G. Di Carlo, M.P. Casaletto, L.F. Liotta, G. Deganello, J. Phys. Chem. B 109 (2005) 2821.
[28] L.F. Liotta, G. Di Carlo, G. Pantaleo, A.M. Venezia, G. Deganello, E. Merlone Borla, M. Pidria, Appl. Catal. B 75 (2007) 182–188.
[29] M. Waqif, P. Bazin, O. Saur, J.C. Lavalley, G. Blanchard, O. Touret, Appl. Catal. B 11 (1997) 193.
[30] L.F. Liotta, G. Di Carlo, G. Pantaleo, A.M. Venezia, G. Deganello, in: Proceedings of the Europacat 8, August 26–31, 2007, Turku, Finland, 2007.
[31] C.-K. Chang, Y.-J. Chen, C.-t. Yeh, Appl. Catal. A 174 (1998) 13.
[32] L.F. Liotta, G. Di Carlo, G. Pantaleo, G. Deganello, Appl. Catal. B 70 (2007) 314.
[33] M.M. Natile, A. Glisenti, Chem. Mater. 15 (2003) 2502.
[34] M.P. Casaletto, A. Longo, A. Martorana, A. Prestianni, A.M. Venezia, Surf. Interface Anal. 38 (2006) 215.
[35] P. Burroughs, A. Hamnett, A.F. Orchard, G. Thornton, J. Chem. Soc. Dalton Trans. 17 (1976) 1686.
[36] G. Jasos, U.M. Graham, E. Chenu, P.M. Patterson, A. Dozier, B.H. Davis, J. Catal. 229 (2005) 499.
[37] Q. Fu, H. Saltsburg, M. Flytzani-Stephanopoulos, Science 301 (2003) 935.
[38] F. Boccuzzi, A. Chiorino, M. Manzoli, T. Tabakova, J. Catal. 188 (1999) 176.
[39] J. El Fallah, S. Boujana, H. Dexpert, A. Kiennemann, J. Majerus, O. Touret, F. Villani, F. Le Normand, J. Phys. Chem. 98 (1994) 5522.
[40] H.Y. Lin, Y.-W. Chen, Mater. Chem. Phys. 85 (2004) 171.
[41] C.-W. Tang, W.-Y. Yu, C.-J. Lin, C.-B. Wang, S.H. Chien, Catal. Lett. 116 (2007) 161.
[42] D. Widmann, R. Leppelt, R.J. Behm, J. Catal. 251 (2007) 437.
[43] J. Jansson, A. Palmqvist, E. Fridell, M. Skoglundh, L. Österlund, P. Thormählen, V. Langer, J. Catal. 211 (2002) 387.
[44] J. Łojewska, A. Kołodziej, J. Żak, J. Stoch, Catal. Today 105 (2005) 655.